Journal of Experimental Botany, Vol. 64, No. 7, pp. 2049–2061, 2013
doi:10.1093/jxb/ert060 Advance Access publication 4 March, 2013
This paper is available online free of all access charges (see http://jxb.oxfordjournals.org/open_access.html for further details)

Journal of Experimental Botany
www.jxb.oxfordjournals.org

RESEARCH PAPER

Rice *SLENDER LEAF 1* gene encodes cellulose synthase-like D4 and is specifically expressed in M-phase cells to regulate cell proliferation

Takanori Yoshikawa[1], Mitsugu Eiguchi[2], Ken-Ichiro Hibara[1], Jun-Ichi Ito[1] and Yasuo Nagato[1]*

[1] Graduate School of Agricultural and Life Sciences, University of Tokyo, 1-1-1, Yayoi, Bunkyo-ku, Tokyo, 113–8657, Japan
[2] National Institute of Genetics, 1111 Yata, Mishima, Shizuoka, 411–8540, Japan

* To whom correspondence should be addressed. Email: anagato@mail.ecc.u-tokyo.ac.jp

Received 6 November 2012; Revised 18 February 2013; Accepted 18 February 2013

Abstract

***Cellulose synthase-like* (*CSL*) genes are predicted to catalyse the biosynthesis of non-cellulosic polysaccharides such as the β-D-glycan backbone of hemicelluloses and are classified into nine subfamilies (*CSLA–CSLH* and *CSLJ*). The *CSLD* subfamily is conserved in all land plants, and among the nine *CSL* subfamilies, it shows the highest sequence similarity to the cellulose synthase genes, suggesting that it plays fundamental roles in plant development. This study presents a detailed analysis of *slender leaf 1* (*sle1*) mutants of rice that showed rolled and narrow leaf blades and a reduction in plant height. The narrow leaf blade of *sle1* was caused by reduced cell proliferation beginning at the P3 primordial stage. In addition to the size reduction of organs, *sle1* mutants exhibited serious developmental defects in pollen formation, anther dehiscence, stomata formation, and cell arrangement in various tissues. Map-based cloning revealed that *SLE1* encodes the OsCSLD4 protein, which was identified previously from a *narrow leaf and dwarf 1* mutant. *In situ* hybridization experiments showed that *OsCSLD4* was expressed in a patchy pattern in developing organs. Double-target *in situ* hybridization and quantitative RT-PCR analyses revealed that *SLE1* was expressed specifically during the M-phase of the cell cycle, and suggested that the cell-cycle regulation was altered in *sle1* mutants. These results suggest that the OsCSLD4 protein plays a pivotal role in the M phase to regulate cell proliferation. Further study of *OsCSLD4* is expected to yield new insight into the role of hemicelluloses in plant development.**

Key words: CSLD, cytokinesis, leaf blade, M-phase, rice, *slender leaf 1*.

Introduction

The plant cell wall plays pivotal roles such as mechanical support, forming a barrier against biotic and abiotic stresses, and control of exchanging materials and signal transduction between cells. The cell wall is composed mainly of polysaccharides, which are classified into cellulose, hemicelluloses, and pectins (Scheller and Ulvskov, 2010). Cellulose microfibrils are the core component of the cell walls, and are typically composed of approximately 36 hydrogen-bonded chains containing 500–14 000 β-1,4-linked glucose molecules (Taylor, 2008). The cellulose synthase (CesA) protein comprises 985–1088 aa, and contains a zinc finger domain at the N terminus, eight transmembrane domains, and a central cytosolic 'catalytic' domain known as the 'D_D_D_QxxRW' motif. It is considered that the CesA complex comprising 36 CesA proteins is embedded in the plasma membrane in hexameric arrays, and that the zinc finger domain at the N terminus participates in the dimerization of CesA proteins (Kurek *et al*., 2002; Taylor, 2008).

Richmond and Somerville (2000) reported a large family of *Cellulose synthase-like* (*CSL*) genes in *Arabidopsis* based on the sequence similarity to *CesA* genes, and classified them into six subfamilies (*CSLA–E* and *CSLG*). Subsequent

Abbreviations: SE, standard error.

© The Author(2) [2013].
This is an Open Access article distributed under the terms of the Creative Commons Attribution Non-Commercial License (http://creativecommons.org/licenses/by-nc/3.0/), which permits unrestricted non-commercial use, distribution, and reproduction in any medium, provided the original work is properly cited.

studies identified three additional *CSL* subfamilies (*CSLF*, *CSLH*, and *CSLJ*) (Hazen *et al*., 2002; Fincher, 2009). Whilst the *CSLB* and *CSLG* subfamilies are found only in dicots, the *CSLF* and *CSLH* subfamilies are specific to grasses, and the *CSLJ* subfamily is found in some angiosperms. The *CSLA*, *CSLC*, and *CSLD* subfamilies are found in all land plants. CSL proteins contain sequence motifs that are characteristic of β-glycosyltransferases. The only difference between CSLs and CesAs is the lack of the zinc finger domains at the N terminus. Most of the CSL proteins appear to be localized in the Golgi, where hemicellulose synthesis takes place. From these characteristics, *CSL* genes are predicted to catalyse the biosynthesis of non-cellulosic polysaccarides such as the β-D-glycan backbone of hemicelluloses (Richmond and Somerville, 2000). This hypothesis is supported by several recent studies, which suggest that the *CSLA* genes encode (gluco)mannan synthases (Liepman *et al*., 2005; Suzuki *et al*., 2006), and that the *CSLF* and *CSLH* genes encode mixed-linkage glucan synthases (Burton *et al*., 2006; Doblin *et al*., 2009). Cocuron *et al*. (2007) suggested that the *CSLC* genes are involved in xyloglucan synthesis. Recently, however, it was reported that some *CSLC* genes of barley are targeted to the plasma membrane, suggesting that the *CSLC* subfamily contains more than one type of polysaccharide synthase (Dwivany *et al*., 2009).

The *CSLD* subfamily genes are commonly found in all land plants, and show the highest similarity to *CesA* family among *CSL* subfamilies at sequence levels (Richmond and Somerville, 2000). To date, six *CSLD* genes have been found in *Arabidopsis*, five in maize, and five in rice (Hunter *et al*., 2012), and several *csld* mutants were identified in these plants. In addition, homology searches have revealed that the *CSLD* subfamily contains three barley genes, five sorghum genes, and six purple false brome genes (Supplementary Fig. S1 at *JXB* online). Phylogenetic analysis revealed that *CSLD* genes are further classified into three clades, which correspond to three classes of their mutant phenotypes (Hunter *et al*., 2012). The first clade includes *AtCSLD1* and *AtCSLD4*, whose mutants show pollen-tube defects (Bernal *et al*., 2008). The second clade comprises *AtCSLD2*, *AtCSLD3*, *OsCSLD1*, and *ZmCSLD5*, and their mutations cause aberrant root-hair development (Favery *et al*., 2001; Wang *et al*., 2001; Kim *et al*., 2007; Bernal *et al*., 2008; Penning *et al*., 2009). The third clade includes *AtCSLD5*, *OsCSLD4*, and *ZmCSLD1*, whose mutants show reduced plant growth (Bernal *et al*., 2007; Li *et al*., 2009; Hu *et al*., 2010; Wu *et al*., 2010; Hunter *et al*., 2012). Whilst expression of the first clade genes *AtCSLD1* and *AtCSLD4* is specific to pollens, the second clade genes *AtCSLD2* and *AtCSLD3* are expressed at the highest levels in root tissues except for the root tips. The third clade gene *AtCSLD5* is expressed at moderate levels in many tissues including root tips and at the highest level in the shoot apex (Bernal *et al*., 2008). These distinct expression patterns among the three clades could correspond to different mutant phenotypes.

The reduced number of cells in *atcsld5* and *oscsld4* mutants and the high expression level of these genes in the meristematic tissues (Bernal *et al*., 2008; Li *et al*., 2009) have suggested a functional relation of *CSLD* to cell proliferation. Recently, Hunter *et al*. (2012) found disrupted cross-wall formation in a *zmcsld1* mutant. As similar phenotypic alterations have frequently been observed in cytokinetic mutants such as *knolle* and *korrigan* in *Arabidopsis* (Lukowitz *et al*., 1996; Zuo *et al*., 2000), it is likely that *ZmCSLD1* is associated with cytokinesis. In addition, Yin *et al*. (2011) revealed that transiently expressed *AtCSLD5* is involved in mannan synthesis in tobacco leaves. The mannosyltransferase activity of *AtCSLD5* was reduced by adding GDP-glucose together with GDP-mannose (Yin *et al*., 2011), suggesting that the *CSLD* subfamily is involved in a different kind of mannan synthesis from that catalysed by the *CSLA* subfamily. Although mannans have been well studied as storage components, little information has been accumulated in relation to cytokinesis.

Here, we present a detailed analysis of rice *slender leaf 1* (*sle1*) mutants that show narrow leaf blades and other developmental abnormalities, the phenotypes being attributable to reduced cell proliferation activity. Map-based cloning revealed that *SLE1* encodes OsCSLD4. This gene is the same as the previously reported *NARROW LEAF AND DWARF 1* (*ND1*) gene (Li *et al*., 2009). The *nd1* mutant showed narrow leaves and reduced plant height. Li *et al*. (2009) revealed the localization of the OsCSLD4 protein in the Golgi. In the present study, we found novel mutant phenotypes that were not described by Li *et al*. (2009), and revealed that *OsCSLD4*/*SLE1* is specifically expressed during the M phase of the cell cycle. These results suggest that the product of *OsCSLD4* plays a pivotal role in the M phase to regulate cell proliferation and plant development.

Materials and methods

Plant materials

Two allelic single-gene recessive mutants of rice (*Oryza sativa* L.) showing distinct rolled and narrow leaf blades and reduced plant height were identified from an M_2 population of *japonica* variety Taichung 65 mutagenized with *N*-methyl-*N*-nitrosourea. We designated these mutants *slender leaf1-1* (*sle1-1*) and *sle1-2*, respectively. For observations at the early vegetative stage, mutants and wild-type seeds were sown on soil and grown at 28 °C under continuous light conditions. Otherwise, plants were grown in pots or in paddy fields under natural conditions.

Epidermal cell observations

The third-leaf blades of *sle1* and wild-type plants were fixed with formaldehyde:glacial acetic acid:50% ethanol (2:1:17) for 24 h at 4 °C. They were then dehydrated in a graded ethanol series. Dehydrated samples were incubated at 96 °C in chloral hydrate dissolved in 100% ethanol until they cleared and were then observed under a light microscope.

Paraffin sectioning and histological analysis

Plant samples of *sle1* and wild-type were fixed with formaldehyde:glacial acetic acid:50% ethanol (2:1:17)) for 24 h at 4 °C for histological analysis, or fixed with 4% (w/v) paraformaldehyde and 1% Triton X in 0.1 M sodium phosphate buffer for 48 h at 4 °C for *in situ* hybridization. They were then dehydrated in a graded ethanol series, substituted with 1-butanol, and embedded

in Paraplast Plus. The samples were sectioned at 8 µm thick using a rotary microtome. For histological analysis, the sections were stained with haematoxylin or calcofluor and observed under a light or fluorescence microscope.

Flow cytometric analysis

Mature leaves of wild-type, *sle1-1*, and *sle1-2* plants were cut into small pieces in 430 µl of extraction buffer (CyStain® UV Precise P), filtered through a 20 µm mesh, and mixed with 1.6 ml of nuclear staining buffer (Partec). The samples were analysed with a Partec Ploidy Analyzer (Partec). For quantification, the mean result of three independent measurements was determined.

In situ hybridization

Paraffin sections were prepared as described above. Digoxigenin-labelled antisense and sense RNA probes were prepared from full-length cDNA of histone *H4* and a 752 bp fragment of *OsCSLD4*/*SLE1*, which was amplified by PCR with forward primer (5′-CAGGGCCTACTCAAGGTGAT-3′) and reverse primer (5′-GCACAGACGTCACACACACA-3′) using genomic DNA as a template. Biotin-labelled antisense and sense RNA probes were prepared from full-length cDNA of *CDKB2;1*. As the sense probes did not give specific signals, only antisense probe data are presented. For single-target *in situ* hybridization, digoxigenin-labelled probes were used. *In situ* hybridization and immunological detection with alkaline phosphatase were performed according to the methods of Kouchi and Hata (1993). The measurement of histone *H4* signal areas in leaf primordia was performed by image analysis with ImageJ (http://rsbweb.nih.gov/ij/). For double-target *in situ* hybridization, a digoxigenin-labelled probe and biotin-labelled probe were used. Hybridization of probes, post-hybridization washes, and blocking procedures were performed according to the methods of Kouchi and Hata (1993). A TSA™ Biotin System (PerkinElmer) together with streptavidin–fluorescein (PerkinElmer) was used for the detection of biotin-labelled probes and an HNPP Fluorescent Detection Set (Roche) was used for the detection of digoxigenin-labelled probes following the manufacturer's protocol. The slides were washed in sterile distilled water and mounted with Prolong Gold Antifade Reagent with DAPI (Invitrogen), and observed with a BZ-8000 fluorescence microscope (Keyence Co.) using GFP band pass, Texas Red, and DAPI band pass filters for fluorescein, HNP/TR, and DAPI signals, respectively.

Map-based cloning

For mapping of the *SLE1* gene, *sle1-1* and *sle1-2* plants were crossed with *indica* variety Kasalath, and F_2 plants showing the *sle1* phenotype were used for mapping. Using cleaved-amplified polymorphic sequence and sequence-tagged site markers, the *SLE1* locus was mapped roughly on the long arm of chromosome 12. The *SLE1* locus was further limited within the region ranged from 78.9 to 91.9 cM. As *OsCSLD4* (*Os12g36890*) located in this region was reported as a causal gene for the *nd1* mutant of rice (Li *et al.*, 2009), we compared the genomic sequence of the gene between *sle1* mutants and wild-type plants.

Quantitative RT-PCR analysis

Total RNA was extracted from whole seedlings using TRIzol reagent (Invitrogen) according to the manufacturer's protocol. After RNase-free DNase (Takara Bio) treatment, 500 ng of total RNA was reverse transcribed with a High Capacity RNA-to-cDNA™ Master Mix (Applied Biosystems) according to the manufacturer's protocol. Quantitative RT-PCR analyses of histone *H4*, *CDKB2;1*, and *UBQ5* were performed using Fast SYBR® Green Master Mix (Applied Biosystems) and quantitative RT-PCR analyses of *SLE1* and *eEF-1a* were performed using TaqMan® Fast Universal PCR Master Mix (Applied Biosystems). Primer sequences used for quantitative RT-PCR were as follows; 5′-CTGATTCCTTCCTTCCTTCCTT-3′ and 5′-CAAATCTTCAGTTCAGATTCATCG-3′ for histone *H4*, 5′-TGATGTTCACCACCAAGGAA-3′ and 5′-TCATTACCATCA CAAACAAGTGAA-3′ for *CDKB2;1*, 5′-ACCACTTCGACCGC CACTACT-3′ and 5′-ACGCCTAAGCCTGCTGGTT-3′ for *UBQ5*, 5′-GAAGCTCACATGAAGGAGTGC-3′ and 5′-CAAACAATCG CTTAATCACACC-3′ for *OsCSLD4*/*SLE1*, and 5′-CGCTCTTCTT GCTTTCACTCTTG-3′ and 5′-TAGGATGAGACTTCCTTCACG ATTTC-3′ for *eEF-1a*. The probe sequences used for quantitative RT-PCR were as follows; 5′-GGCGTGTTGTCAAATTCAGTT-3′ for *SLE1* and 5′-CAACAAGATGGATGCCAC-3′ for *eEF-1a*. The *SEL1* probe was labelled with FAM and TAMRA, and the *eEF-1a* probe was labelled with FAM and NFQ-MGB. Quantitative RT-PCR analysis was performed using the StepOnePlus™ Real-Time PCR System (Applied Biosystems).

Results

We identified two alleles of *SLE1*: *sle1-1* and *sle1-2*. As several phenotypes of *SLE1* have already been described by Li *et al.* (2009), we focused on a detailed observation of the developmental process in the mutant. We also found an abnormality in the reproductive phase that was not described by Li *et al.* (2009).

Phenotypes of sle1 mutants in the vegetative phase

Both *sle1-1* and *sle1-2* showed rolled and narrow leaf blades (Fig. 1A, B). The width of the leaf blade was reduced to about 60% of that of the wild type, and this trend was observed in all leaves (Fig. 1C, D). The length of the leaf blade was also reduced, although it was less severe than the reduction in width (Fig. 1E, F). To compare the epidermal cells in the leaf blades, we cleared the third leaves of wild-type and *sle1* mutant plants with chloral hydrate (Fig. 1G). On the abaxial surface, no significant difference was observed in the width of the intercostal epidermal cells, but the length of the intercostal epidermal cells in the *sle1* mutants was 20% greater than in the wild type (Fig. 1H). A similar trend was also observed in the cork cells of costal cells in the third-leaf blades (Supplementary Fig. S2 at *JXB* online). In the *sle1* mutant, the total number of cells along the leaf width was reduced by approximately 40%, and along the leaf length, it was reduced by approximately 30% compared with the wild type (Fig. 1I). Thus, the short and narrow leaves of *sle1* mutants were caused by a defect in cell proliferation. Concomitant with the leaf size, *sle1* mutants also showed a dwarf phenotype at maturity due to a reduction in the lengths of the two uppermost internodes (Supplementary Fig. S3 at *JXB* online). Abnormalities were also observed in the belowground plant parts. The roots of the *sle1* mutants were more slender and shorter compared with those of the wild type, and the number of crown roots was decreased in the mutants (Supplementary Fig. S4 at *JXB* online). The *sle1* mutants also exhibited poor development of lateral roots and root hairs (Supplementary Fig. S4).

We investigated the early leaf development of *sle1* plants to determine when leaf reduction begins in the mutant.

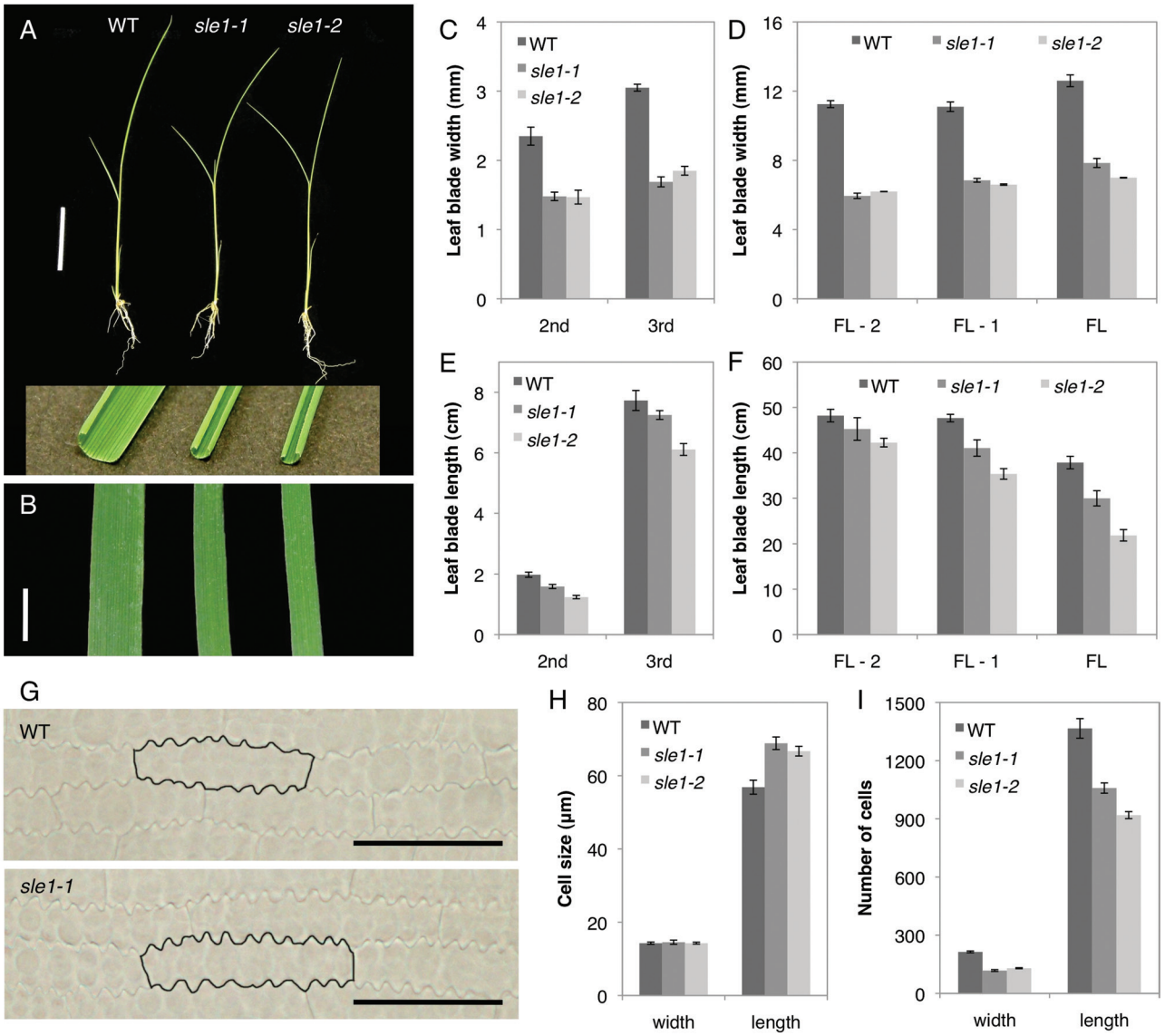

Fig. 1. Vegetative phenotypes of wild-type, *sle1-1*, and *sle1-2* plants. (A) Fourteen-d-old seedlings of wild-type, *sle1-1*, and *sle1-2* plants. Sections of the third-leaf blades are shown in the inset. (B) Mechanically unrolled third-leaf blades of wild-type, *sle1-1*, and *sle1-2* plants (left to right). Bars, 5 cm (A), 3 mm (B). (C–F) Comparison of width (C, D) and length (E, F) of leaf blades among wild-type, *sle1-1*, and *sle1-2* plants. Results for the second and third leaves are shown, and for the flag leaf (FL) and leaves one and two lower than the flag leaf (FL-1 and FL-2, respectively). Results are shown as means ±standard error (SE) (n=10). (G) The abaxial surface of the third-leaf blade of wild-type and *sle1-1* plants. The representative cells are outlined in black. Bars, 50 μm. (H, I) Comparison of epidermal cell size (H) and number of cells (I) in the third-leaf blade among wild-type, *sle1-1*, and *sle1-2* plants. To estimate the number of cells comprising the third-leaf blade, the width and length of the leaf blade were divided by those of epidermal cells. Results are shown as means ±SE (n=5). (This figure is available in colour at *JXB* online.)

Although the width of the late P2 leaf primordium in *sle1* plants was comparable to that of the wild type (Fig. 2A, E, I), *sle1* plants already exhibited narrower leaf blades in the early P3–P5 leaf primordia (Fig. 2B–D, F–I). To determine the cause of leaf narrowness in *sle1* plants, we estimated the number of epidermal cells in the width direction of the third-leaf blade. Although the number of cells did not largely differ at the late P2 stage, *sle1* plants showed significantly fewer cells from the early P3 stage (Fig. 2J). On the other hand, epidermal cell width did not largely differ between *sle1* and wild-type plants (Fig. 2K). These results indicated that the narrow leaves of *sle1* mutants are caused mainly by impaired cell proliferation. To confirm the impaired cell proliferation in *sle1* mutants, we used *in situ* hybridization to examine the expression of histone *H4*, which is expressed specifically in S-phase cells (Fig. 3A–D). For quantitative evaluation, the relative number of cells expressing histone *H4* was calculated using ImageJ software. The frequency of cells expressing histone *H4* was reduced in both P2 and P3 leaf primordia in *sle1-1* plants (Fig. 3E) relative to the wild type, indicating that the narrow leaf blade of *sle1* plants is caused by impaired cell proliferation at an early stage.

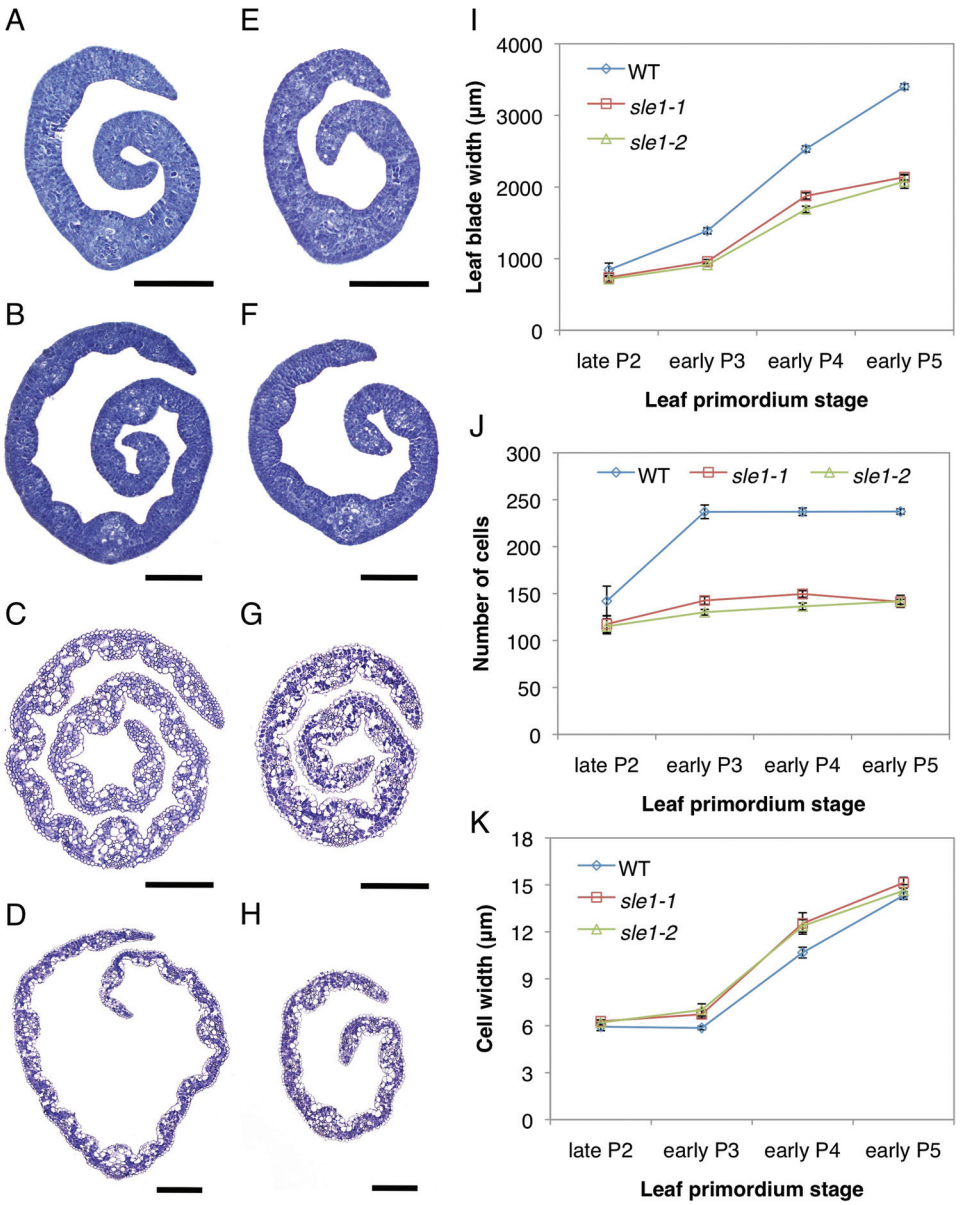

Fig. 2. Development of the third-leaf blade in wild-type, *sle1-1*, and *sle1-2* plants. (A, E) Cross-sections of late P2 leaf blades in wild-type (A) and *sle1-1* (E) plants. (B, F) Cross-sections of early P3 leaf blades in wild-type (B) and *sle1-1* (F) plants. (C, G) Cross-sections of early P4 leaf blades in wild-type (C) and *sle1-1* (G) plants. (D, H) Cross-sections of early P5 leaf blades in wild-type (D) and *sle1-1* (H) plants. Bars, 100 μm (A, B, E, F); 200 μm (C, D, G, H). (I) Increase in the third-leaf blade width at the early stages in wild-type, *sle1-1* and *sle1-2* plants. (J) Number of epidermal cells in the width direction at the early stages in the third-leaf blade. (K) Epidermal cell width at the early stages in the third-leaf blade. Leaf blade width was calculated from the cross-sections of leaf primordium at each stage using ImageJ software. The widths of epidermal cells in late P2 and early P3 leaf primordium were calculated from the longitudinal sections of leaf blade, and those in early P4 and P5 leaf primordium were calculated from the cleared leaf blade (see Materials and methods) using ImageJ software. To estimate the number of cells, the leaf blade width was divided by the mean epidermal cell width. Results are shown as means ±SE (n=3). (This figure is available in colour at *JXB* online.)

Phenotypes of sle1 mutants in the reproductive phase

The *sle1* mutants showed distinct abnormalities at the reproductive stage, which have not been described in detail previously. The panicles of *sle1* mutants were shorter than those of the wild type (Fig. 4A, Table 1). The number of spikelets per panicle was significantly reduced due primarily to a decreased number of primary branches (Table 1). The slender leaf phenotype was also reflected in the spikelets; spikelet width in *sle1* plants was significantly reduced, while the spikelet length was comparable to that of wild type (Table 1). Presumably, these reductions in both the number and width of spikelets can be attributed to the defect in cell proliferation. One of the most striking features of the *sle1* panicles was low seed fertility (approximately 30% in *sle1* plants compared with >90% in the wild type).

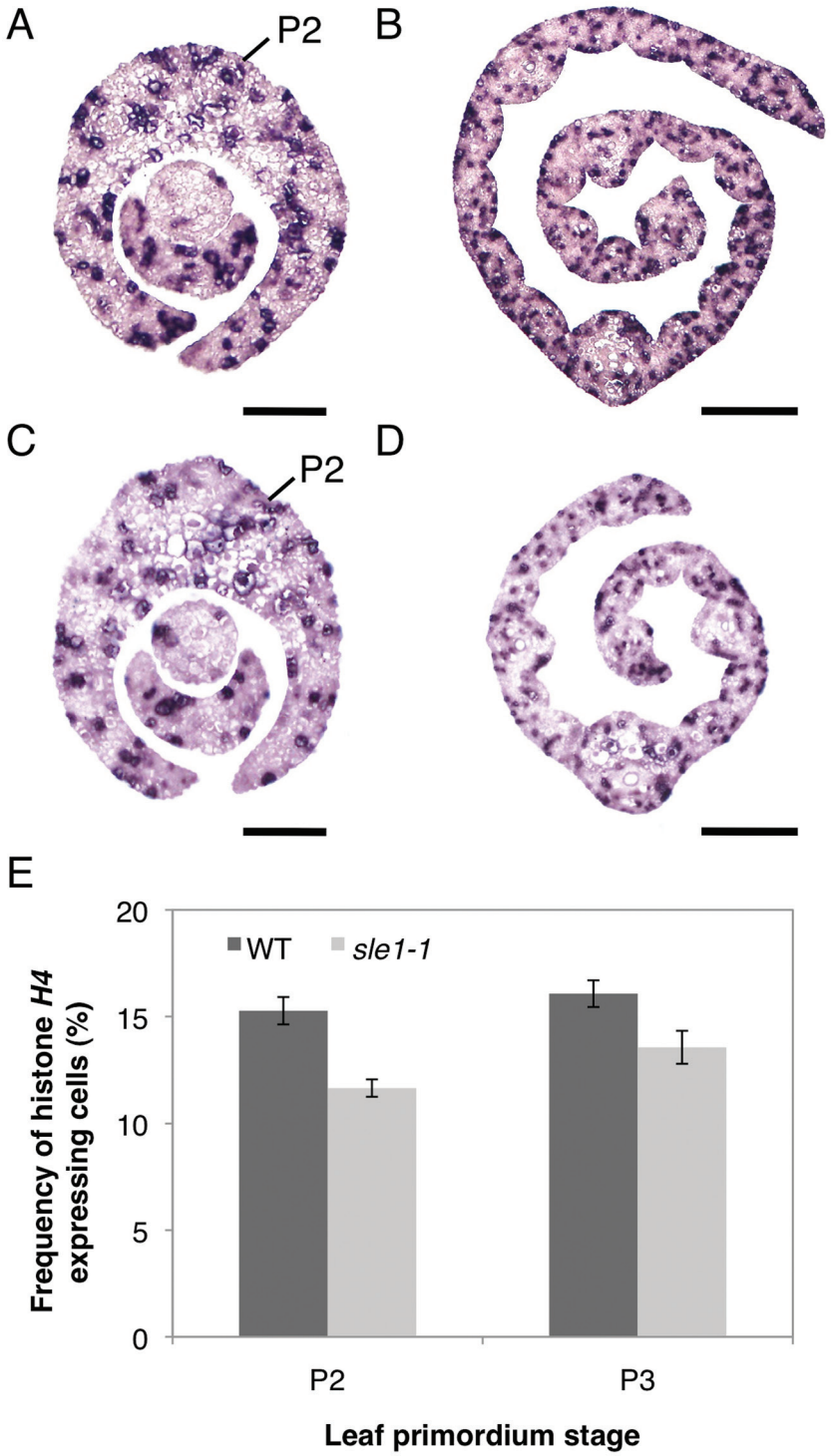

Fig. 3. Expression patterns of histone *H4* in P2 and P3 leaf primordia in wild-type and *sle1-1* plants. Ten-d-old seedlings were used. (A, C) Cross-sections of P2 leaf primordia in wild-type (A) and *sle1-1* (C) plants. (B, D) Cross-sections of a P3 leaf blade in wild-type (B) and *sle1-1* (D) plants. Bars, 50 μm (A, C); 100 μm (B, D). (E) Frequency of histone *H4*-expressing cells in P2 and P3 leaf primordia. Results are shown as means ±SE (n=6). (This figure is available in colour at *JXB* online.)

Therefore, many of the spikelets remained green when the seeds matured (Fig. 4A). To discover the reason for this low fertility, we first observed the ovules of *sle1* mutants, but no significant phenotypic alteration was detected. Furthermore, *sle1* plants could set seeds when crossed with wild-type plants, eliminating the pistils as the cause of low fertility. We then examined the dehiscence of the anthers. In wild-type plants, dehiscence occurred at flower opening and the stigmas were covered with many pollen grains (Fig. 4B, D), whereas in *sle1* mutants, few anthers dehisced

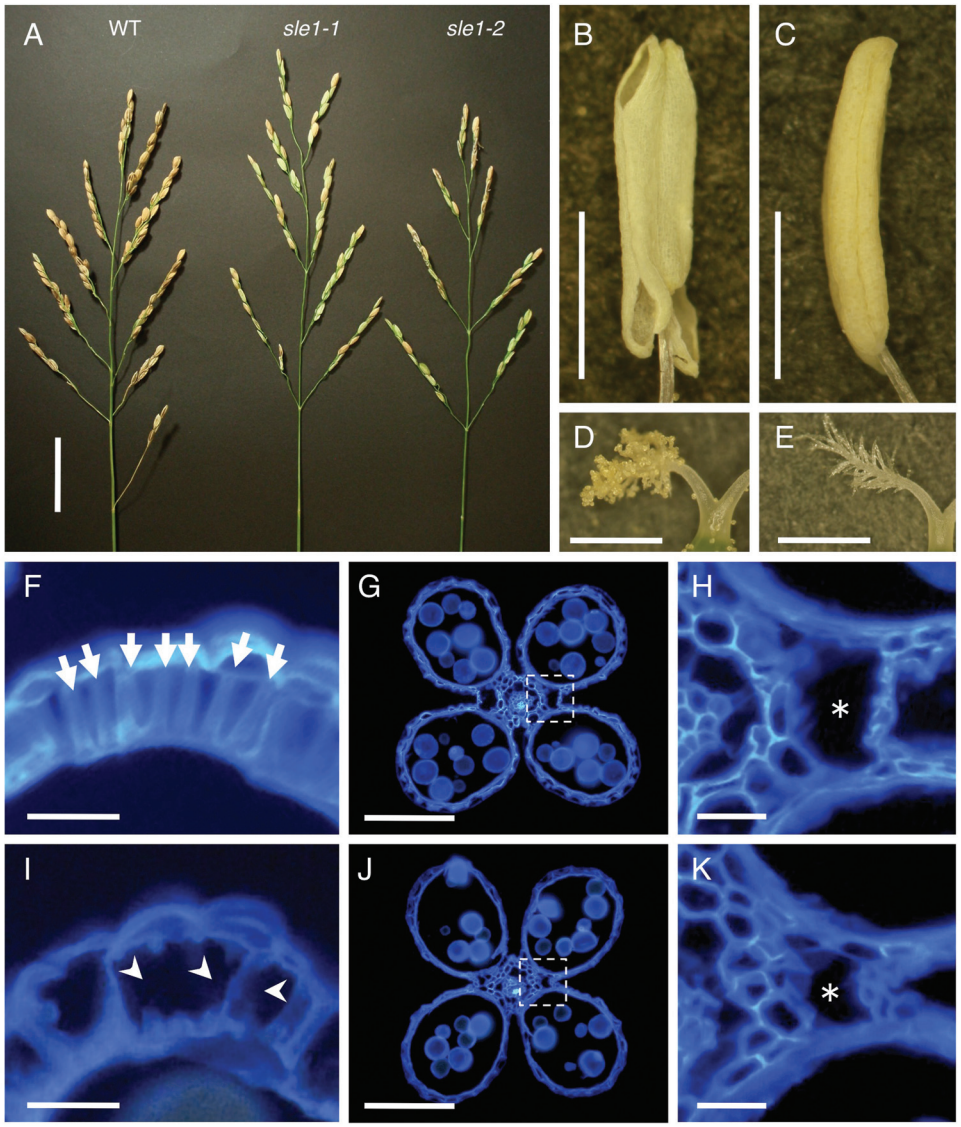

Fig. 4. Reproductive phenotypes of wild-type, *sle1-1*, and *sle1-2* plants. (A) Panicles of wild-type, *sle1-1*, and *sle1-2* plants. (B–E) Anthers and stigmas of wild-type (B, D) and *sle1-1* (C, E) plants at flower opening. The anthers were well dehisced in wild-type plants (B), but anther dehiscence was hardly observed in *sle1* plants (C). Numerous pollen grains are attached to the stigmas in wild-type plants (D), with only a few attached on the *sle1* stigma (E). (F–K) Cross-sections of anthers in wild-type (F, G) and *sle1-1* (I, J) plants stained with calcofluor. (F) and (I) are sections of the upper part of the anther. In (F), the arrows indicate normal fibrous structures formed in endothecium cells. In (I), the fibrous structures in the endothecium cells were partly lost (arrowheads) in *sle1-1* plants. (G) and (J) are sections of the middle part of the anther. (H) and (K) show close-up views of the boxed regions in (G) and (J), respectively. Asterisks indicate cavities for dehiscence. Bars, 5 cm (A); 1 mm (B–E); 10 μm (F, H, I, K); 100 μm (G, J).

and few pollen grains was observed on the stigmas (Fig. 4C, E). Therefore, poor dehiscence of anthers appeared to be the major cause of low seed fertility in the *sle1* mutants. The driving force for anther dehiscence normally arises from fibrous structures in the endothecium cells, along with the development of cavities and the rupture of septa that are indispensable for dehiscence (Matsui *et al.*, 1999). In the *sle1* mutants, development of both the fibrous structures in the endothecium cells and the necessary cavities for dehiscence was incomplete (Fig. 4F–K). Thus, the *SLE1* gene is also involved in the development of these structures.

The sle1 mutant is defective in cell division and cell size/shape regulation

The *sle1* mutants showed pleiotropic abnormalities in pollen formation, anther dehiscence, stomata formation, and cell arrangement in various tissues, as well as altered organ size. In the leaf blades, bulliform cells and bundle-sheath cells were enlarged, but the vascular bundles were smaller than those of the wild type (Fig. 5A, B). In addition, the number of vascular bundles in the leaf blades was significantly reduced in the *sle1* mutants, whilst the distance between vascular bundles

Table 1. Summary of panicle traits in wild-type and *sle1* plants. Values indicate the mean of ten samples ±SE. Asterisks indicate results that were significantly different from the wild type (WT) at P <0.05 (*) and P <0.01 (**) (t-test).

	Panicle length (cm)	No. of primary branches per panicle	No. of spikelets per panicle	Spikelet length (mm)	Spikelet width (mm)
WT	21.9±0.7	10.8±0.4	114.3±8.8	7.6±0.1	3.7±0.05
sle1-1	18.9±0.5**	7.0±0.6**	57.5±4.5**	7.7±0.2	2.9±0.04**
sle1-2	15.1±0.6**	6.4±0.4**	40.0±3.2**	8.0±0.1*	3.1±0.03**

was not affected (Supplementary Fig. S5 at *JXB* online). In the leaf sheath of the *sle1* mutant, the cells were apparently enlarged, together with a reduction in cell number (Fig. 5C, D). The stomata were sometimes ill formed (Fig. 5E, F), and occasionally enlarged cells of unknown identity were observed in the stomatal lineage (Fig. 5G). As these cells were always positioned where the stomata should have been formed, these cells appeared to be abnormal stomata cells, suggesting that improper cell divisions may have taken place in the course of stomata development. Occasionally, anthers showed abnormal development, and many of the pollen grains in such anthers were also misshapen in the *sle1* mutants (Fig. 5H–J). Thus, the *SLE1* mutation affected not only the cell number and size but also the cell shape and tissue differentiation.

The SLE1 gene encodes OsCSLD4

Map-based cloning using an F_2 population from *sle1-1*, *sle1-2*, and ssp. *indica* variety Kasalath revealed that *SLE1* encodes

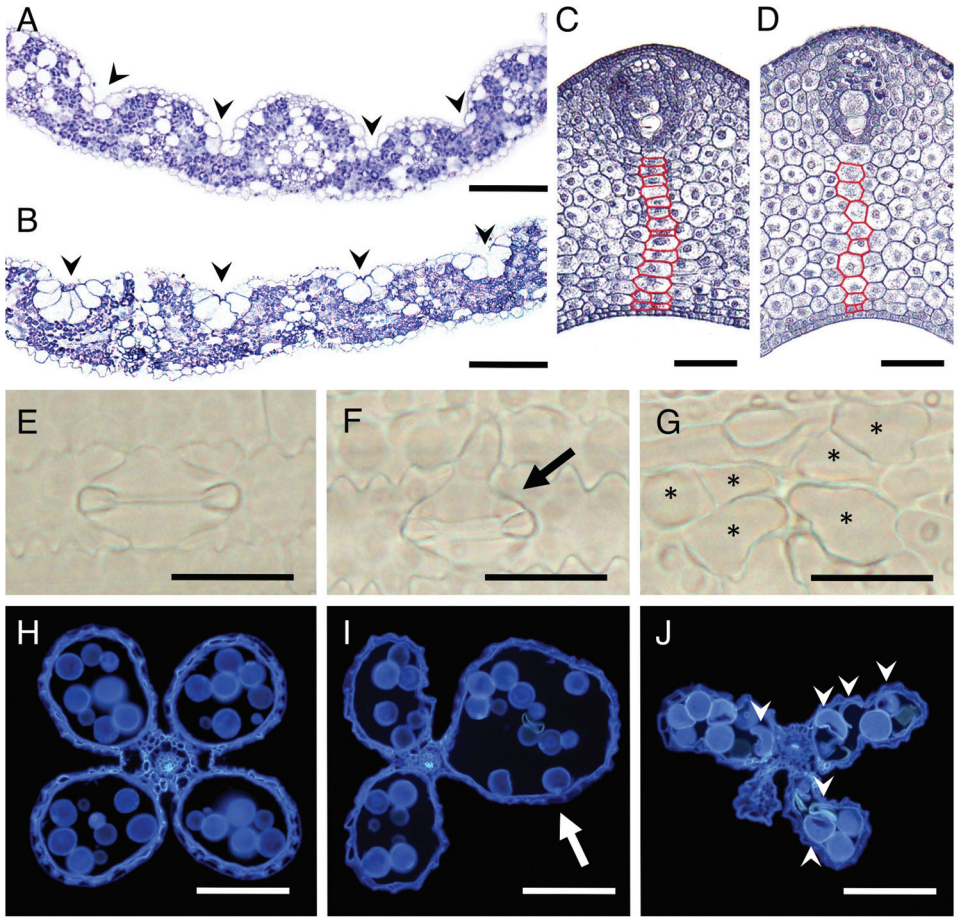

Fig. 5. Abnormal cell division and wide variation in cell size/shape in *sle1* tissues. (A, B) Cross-sections of the third-leaf blades in wild-type (A) and *sle1-1* (B) plants. Arrowheads indicate the positions of bulliform cells. (C, D) Cross-sections of the leaf sheath of P4 leaf primordia in wild-type (C) and *sle1-2* (D) plants. Along the representative cell file (indicated in red) extending from the vascular bundle to the adaxial epidermis, there were 16 cells in the wild-type plant, but only ten cells in the *sle1-2* plant. (E–G) Stomata in wild-type (E) and *sle1-2* (F) plants. The arrow in (F) indicates an abnormal stomata. The asterisks in (G) indicate enlarged cells at the position where stomata should be formed. (H–J) Cross-sections of anthers in wild-type (H), *sle1-1* (I), and *sle1-2* (J) plants. The arrow in (I) indicates an abnormal pollen sac and the arrow heads in (J) indicate defective pollen grains. Bars, 100 μm (A, B, H–J); 50 μm (C, D); 25 μm (E–G).

OsCSLD4, which is identical to the previously reported ND1 protein (Li *et al*., 2009) (Fig. 6A). The OsCSLD4 protein contains a 'D_D_D_QxxRW' motif with two and six transmembrane domains at the N- and C-terminal regions, respectively. In *sle1-1*, a 44 bp fragment ranging from nt 887 to 930 was deleted, which caused a frameshift with concomitant loss of function of all of the transmembrane domains and central motif. In addition to the above deletion, a single-nucleotide substitution from G to A at nt 961 occurred in *sle1-1* plants. In *sle1-2* plants, a nucleotide was substituted from C to A at nt 2960, which caused an amino acid substitution from Ser to Tyr in the third transmembrane domain from the N terminus. This Ser is conserved throughout CesA and all CSLD proteins in rice (Fig. 6B). Therefore, this amino acid substitution conceivably could impair the function of this transmembrane domain and affect the function of the OsCSLD4 protein.

OsCSLD4/SLE1 is expressed during the M phase of the cell cycle

Using RT-PCR and a promoter–β-glucuronidase construct, Li *et al*. (2009) showed that *OsCSLD4*/*SLE1* was expressed primarily in rapidly growing tissues. To determine cell types in which *OsCSLD4* is expressed, we examined the detailed expression pattern of *OsCSLD4* by *in situ* hybridization. No signals were detected when we used a sense probe of *OsCSLD4*, so only results obtained using an antisense probe are described here. The *OsCSLD4* transcripts were detected in actively developing tissues, such as the shoot apex and root tip (Fig. 6C, D), in agreement with Li *et al*. (2009). However, the expression in any given tissue was not uniform but patchy; i.e. within a tissue, the *OsCSLD4*-expressing cells were dispersed (Fig. 6C, D). This patchy expression pattern suggests that *OsCSLD4* expression is associated with the cell cycle, similar to the S-phase-specific histone *H4* or the (G2-)M-phase-specific *CDKB2;1* (Umeda *et al*., 1999). Therefore, we performed a double-target *in situ* hybridization of *OsCSLD4* counterstained with histone *H4* or *CDKB2;1*. Cells expressing *OsCSLD4* did not coincide with those expressing histone *H4* (Supplementary Fig. S6 at *JXB* online), but coincided with those expressing *CDKB2;1* (Fig. 7A–C), indicating that *OsCSLD4* is expressed in M-phase cells. The signals of *OsCSLD4* could be observed in prophase, metaphase, and anaphase cells (Fig. 7D–S), suggesting that *OsCSLD4* was expressed throughout the M phase.

Next, we re-evaluated the mutant phenotypes in light of the observed specific expression of *OsCSLD4* in M-phase

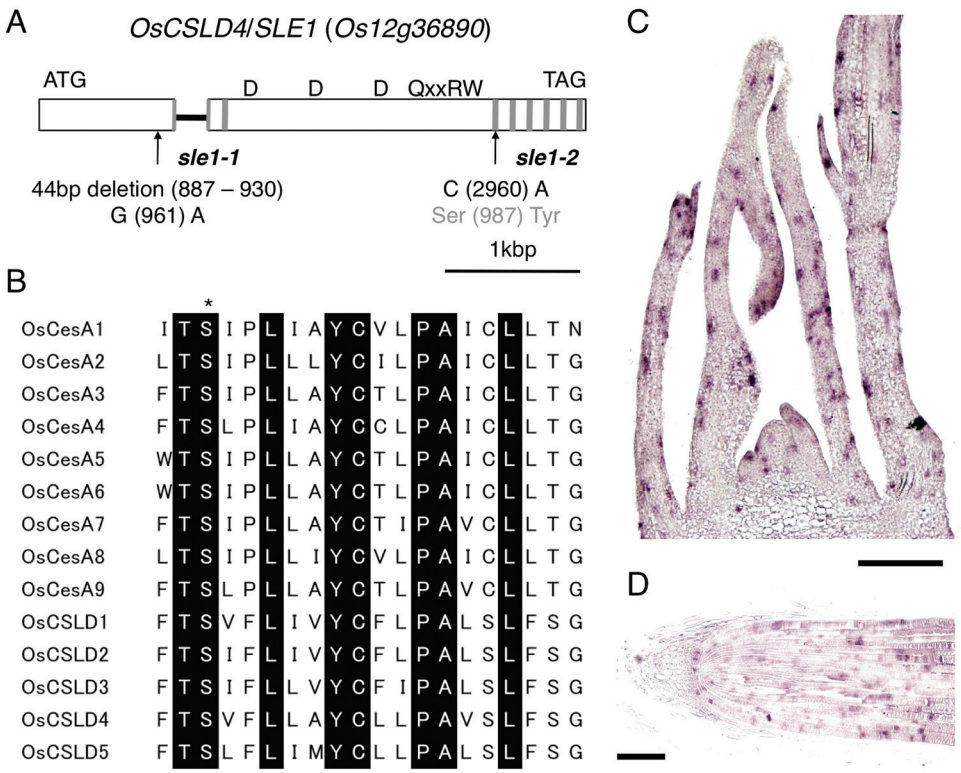

Fig. 6. Structure of the *OsCSLD4*/*SLE1* gene, alignment of the third transmembrane domain from the N terminus of *CesA* and *CSLD* genes in rice, and expression pattern of *OsCSLD4.* (A) Structure of the *OsCSLD4* gene (*Os12g36890*). Open boxes represent exons, and the filled bar represents the intron. Transmembrane domains are represented by grey boxes (the first transmembrane domain from the N terminus is split by the intron). The central domain is represented by 'D_D_D_QxxRW'. Arrows indicate the positions of the *sle1-1* and *sle1-2* mutations, respectively. (B) Alignment of amino acid sequences in the third transmenbrane domains in rice CesA and CSLD proteins. Amino acids conserved in all genes are represented by black boxes. The mutated residue in the *sle1-2* mutant is indicated by an asterisk. (C, D) *In situ* hybridization of *OsCSLD4* in longitudinal sections of 10-d-old shoot apex (C) and root tip (D). Bars, 100 μm. (This figure is available in colour at *JXB* online.)

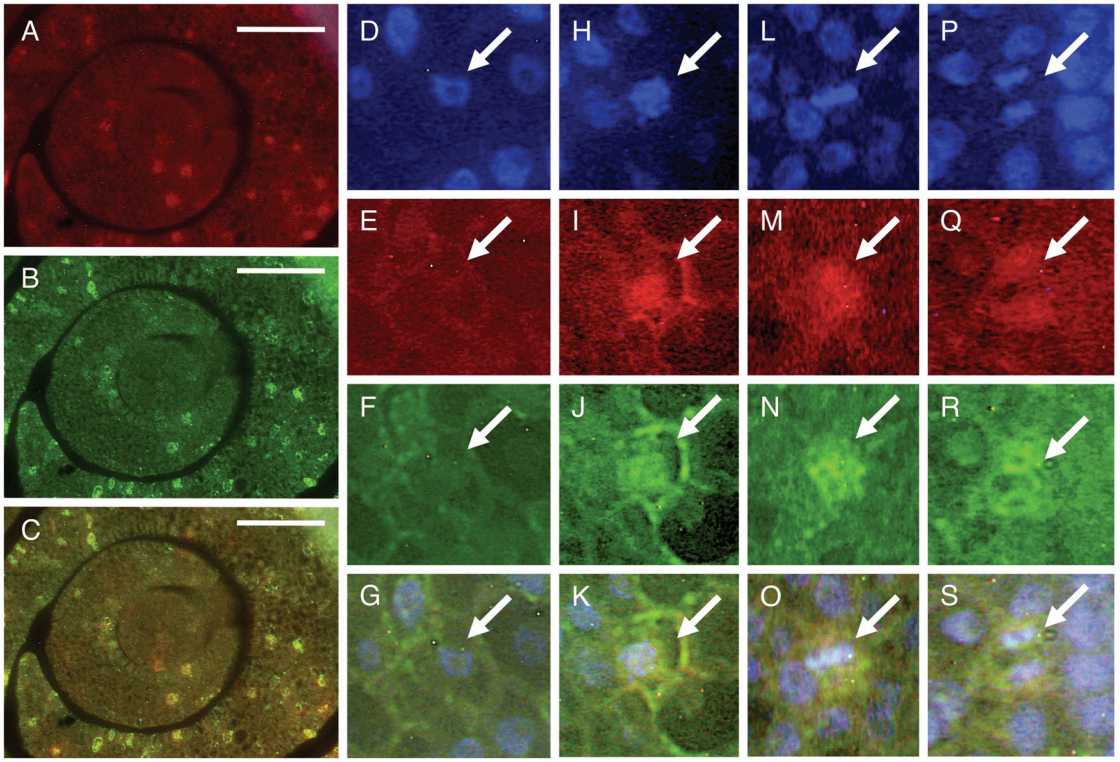

Fig. 7. Double-target *in situ* hybridization of *OsCSLD4* and *CDKB2;1* in the shoot apex of wild-type plants. Ten-d-old seedlings were used. (A–C) Cross-sections of the shoot apex. Bars, 50 μm. (D–S) Results are shown for interphase (D–G), prophase (H–K), metaphase (L–O), and anaphase (P–S) cells, respectively. Arrows indicate the representative cells. Expression patterns of *OsCSLD4* (A, E, I, M, Q) and *CDKB2;1* (B, F, J, N, R) are shown, together with DAPI staining (D, H, L, P). Merged views of (A and B), (D–F), (H–J), (L–N), and (P–R) are shown in (C), (G), (K), (O), and (S) respectively.

cells. In Fig. 3, we showed decreased expression of histone *H4* in *sle1* mutants, suggesting a reduced frequency of S-phase cells. Therefore, we examined the expression of *CDKB2;1* and *OsCSLD4* in the *sle1* mutants. *OsCSLD4* signals were detected in *sle1* cells expressing *CDKB2;1*, indicating that the M-phase specificity of *OsCSLD4* expression was not altered in the *sle1* mutants (Fig. 8A–F). However, the number of signals of both *OsCSLD4* and *CDKB2;1* increased in the *sle1* mutants (Fig. 8G). To quantify gene expression, we performed quantitative RT-PCR analyses of histone *H4*, *CDKB2;1*, and *OsCSLD4* in wild-type and *sle1* plants (Supplementary Fig. S7 in *JXB* online). The expression levels of histone *H4* were reduced in *sle1* plants, in agreement with Fig. 3. However, the expression of *CDKB2;1* and *OsCSLD4* was significantly enhanced in the *sle1* mutants, in agreement with Fig. 8A–G. These results indicated an altered cell-cycle regulation in *sle1* mutants, which could be responsible for the reduced cell proliferation and enlarged cell size in these plants.

The above results suggest the possibility that cytokinesis is affected in the *sle1* mutant, and thus that *sle1* mutant has defects in cell division. Therefore, we measured the DNA content in mature leaf blade cells by flow cytometry. All the wild-type leaf-blade cells had 2C-DNA (diploid). In contrast, although most of *sle1* cells had 2C-DNA, a small number of *sle1* cells showed 4C-DNA (tetraploid; Fig. 8H). These tetraploid cells suggested that incomplete cytokinesis may take place in *sle1* mutants.

Therefore, we concluded that *OsCSLD4*/*SLE1* plays a pivotal role in cell proliferation and plant development via regulation of M-phase progression.

Discussion

We identified the causal gene of the *sle1* mutation, which causes pleiotropic abnormalities such as narrow leaves, as *OsCSLD4*, which was reported previously by Li *et al.* (2009). The *OsCSLD4* gene was expressed specifically during the M phase of the cell cycle (Fig. 7), and the *sle1* mutation in *OsCSLD4* apparently caused an alteration in cell-cycle regulation: the frequency of S-phase cells was reduced in *sle1* mutants in agreement with the impaired cell proliferation, whereas the frequency of M-phase cells was increased significantly (Fig. 3, Fig. 8A–G, Supplementary Fig. S7). Therefore, these results implied that progression of the M phase is disturbed by the loss of SLE1 function, and the prolonged M phase resulted in a prolonged cell cycle, which would be responsible for the impaired cell proliferation and relatively short S phase in *sle1* mutants. In addition, the *sle1* mutation affected not only the cell number and size but also the cell shape, and tissue differentiation (Fig. 5). Thus, *OsCSLD4* plays a pivotal role in plant development.

Several studies have suggested a conserved function of *CSLD* genes in plants, and reduced cell proliferation has been

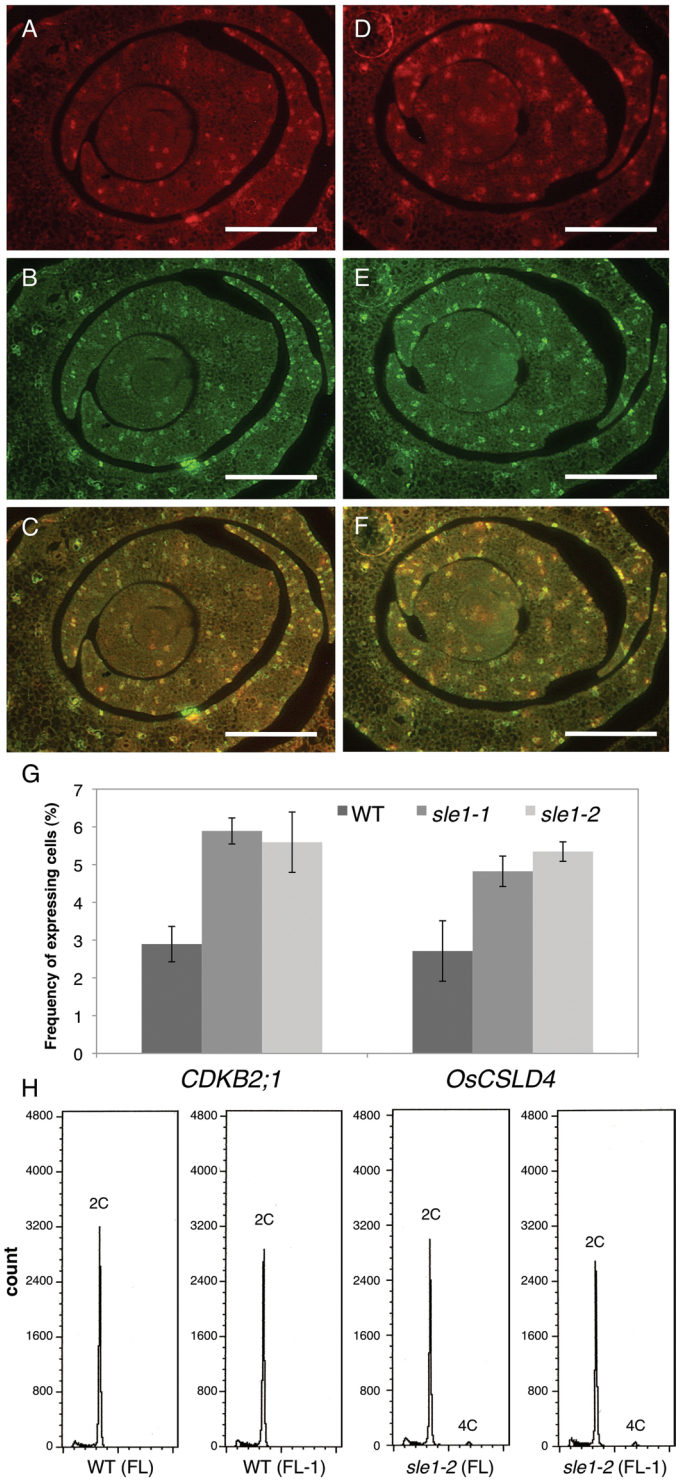

Fig. 8. Expression of *OsCLSD4/SLE1* and *CDKB2;1*, and measurement of DNA content in *sle1* plants. (A–F) Double-target *in situ* hybridization of *OsCLSD4/SLE1* counterstained with *CDKB2;1* in cross-sections of wild-type and *sle1-2* shoot apices. Ten-d-old seedlings were used. (A–C) Wild-type plants. (D–F) *sle1-2* plants. (A, D) Expression pattern of *OsCSLD4*. (B, E) Expression pattern of *CDKB2;1*. (C, F) Merged views of (A and B) and (D and E), respectively. Bars, 100 μm. (G) Frequency of *CDKB2;1*- and *OsCSLD4*-expressing cells in P2 leaf primordia. Results are shown as means ±SE (n=3). (H) Flow cytometric measurement of DNA content in mature leaf-blade cells of wild-type and *sle1-2* plants. FL and FL-1 indicate the flag leaf and one leaf lower than the flag leaf, respectively.

reported in *atcsld5*/*oscsld4*/*zmcsld1* mutants (Bernal *et al.*, 2007; Li *et al.*, 2009; Hu *et al.*, 2010; Wu *et al.*, 2010; Hunter *et al.*, 2012). In this study, we suggest that the reduced cell proliferation might be attributable to the prolonged M phase in *sle1* mutants. Similar results were obtained in a maize *zmcsld1* mutant in which cells with 4C nuclei were detected with high frequency (Hunter *et al.*, 2012). In a preliminary examination of the expression pattern of *AtCSLD5*, an *Arabidopsis* orthologue of *OsCSLD4*, we saw by *in situ* hybridization that *AtCSLD5* was expressed in developing organs in a similar patchy pattern as *OsCSLD4* (Supplementary Fig. S8). Menges *et al.* (2003) performed microarray analysis using synchronized cell suspensions of *Arabidopsis* and suggested that *AtCSLD5* expression occurred at M phase. Therefore, it is considered that the molecular function of the *CSLD* genes is conserved among rice, maize, and *Arabidopsis*.

Malformations of cells were typically observed in the stomata formation in *sle1* plants (Fig. 5E–G). Stomata are normally formed by three highly coordinated cell divisions after the establishment of stomatal cell files in immature leaves (Kamiya *et al.*, 2003). Malformations of stomata have also been observed in cytokinetic mutants (Söllner *et al.*, 2002). As the cell-cycle regulation is impaired in *sle1* mutants, it is plausible that the abnormal stomata in *sle1* leaves resulted from improper timing of cell division in the course of stomata development. We also observed abnormally enlarged and malformed cells in the leaves and anthers of *sle1* (Fig. 5A–D, H–J). A *zmcsld1* mutant was shown to have defective cross-wall formation (Hunter *et al.*, 2012). Such phenotypic alterations have been observed frequently in cytokinetic mutants of *Arabidopsis*, such as *knolle*, *korrigan*, and *hinkel* (Lukowitz *et al.*, 1996; Zuo *et al.*, 2000; Strompen *et al.*, 2002). In these mutants, impairment of cytokinesis was often caused by a failure of cell-plate formation. Thus, we speculate that failure of cell-plate formation may have caused the abnormal cells that we observed in the *sle1* mutants. This proposition is supported by the presence of 4C cells in the *sle1* leaf blade (Fig. 8H). Although the frequency of cells containing 4C-DNA was low, as endoduplication does not occur in normal rice leaf blade, it is probable that in *sle1* leaf blade, impaired cell-plate formation eventually results in the failure of cytokinesis and formation of a 4C nucleus by nuclear fusion (Klindworth and Williams, 2001).

During cytokinesis, Golgi-derived vesicles containing cell-wall materials are transported to the equatorial zone, where they fuse rapidly from the centre of the equatorial zone to form the cell plate (Samuels *et al.*, 1995). The *CSLD* subfamily is considered to function in the synthesis of polysaccharides, particularly mannan (Yin *et al.*, 2011), and the OsCSLD4/AtCSLD5 proteins are localized in the Golgi apparatus (Bernal *et al.*, 2007; Li *et al.*, 2009). These observations, along with our results that *OsCSLD4* is expressed specifically in M-phase cells, suggest the possibility that *OsCSLD4* is involved in cell-plate formation.

In addition to a reduction in leaf size and plant height, we also observed poor dehiscence of anthers in *sle1* plants (Fig. 4B–E), mainly due to the poor development of fibrous structures in the endothecium cells and underdeveloped cavities for dehiscence (Fig. 4F–K). Aberrant anthers were observed

occasionally in the *sle1* mutants, and many of the pollen grains in these anthers were defective (Fig. 5H–J). Similar phenotypic alterations in anthers and pollen grains are caused by environmental stresses such as drought stress (Ji *et al*., 2011). Rice is the most drought-sensitive plant among the major cereal crops, and reproductive development is especially susceptible to drought stress. Because the *sle1* mutants exhibited a distinct rolled-leaf phenotype, which is a common dehydration-avoidance mechanism in rice, the *sle1* mutants may also have experienced drought stress to some extent, presumably because of the impaired development of roots (Supplementary Fig. S4). Another possible mechanism for the defective anthers and pollen grains in *sle1* plants is an abnormality in meiosis. Zhou *et al*. (2011) described a *pollen semi-sterility1* (*pss1*) mutant, which displayed defective anther dehiscence and reduced pollen viability due to defective male meiosis. The phenotypic similarity between *sle1* and *pss1* also suggests the possibility of an impairment in meiosis in the *sle1* mutant. From these phenotypic alterations, *sle1* is clearly involved not only in cell proliferation but also in proper plant development.

The reduction in leaf-blade width was attributable to the reduction in cell number in the *sle1* mutants (Fig. 1I). The narrow leaf blade phenotype was apparent as early as the P3 primordium (Fig. 2I), and cell proliferation activity decreased in P2 and P3 primordia (Fig. 2J, Fig. 3). Although the number of cells in the leaf sheaths of *sle1* was reduced, the cells were enlarged, keeping the shape of the leaf sheaths less altered (Fig. 5C, D). Plants are able to compensate for a reduction in cell number by an increase in cell size (Horiguchi and Tsukaya, 2011). Therefore, these cellular enlargements in the *sle1* leaf sheath may be attributable partly to impaired cell proliferation. Similar compensation was also observed along the length of the leaf blade, in which the reduction in cell numbers was partially compensated by a 20% enlargement of the cell length compared with that of the wild type (Fig. 1H). Along the width of the leaf blade, however, no distinct compensation was observed in the epidermal cells, i.e. the cell width was not altered despite a reduced number of cells across the width of the leaf. Therefore, the degree of compensation may differ depending on the organ and/or the direction, and the phenotypic alteration of *sle1* mutants was apparently affected by such a heterogeneous compensation.

The *CSLD* subfamily genes exhibit the most ancient intron/exon structure, and the wide distribution of *CSLD* genes across all land plant taxa implies a highly conserved function of this subfamily of proteins (Richmond and Somerville, 2000). In this study, we have presented evidence that *OsCSLD4* is required for proper cell division and proliferation during the M phase of the cell cycle. These results reinforce the fundamental function of *CSLD* genes in plant development. Söllner *et al*. (2002) concluded that certain aspects of cytokinesis and root-hair morphogenesis might be regulated by the same molecules. Therefore, it is probable that the product of the CSLD subfamily is involved not only in tip growth but also in cell proliferation. In fact, the root-hair defect in the *Atcsld3* mutant could be rescued partly by introducing *35S:YFP-AtCSLD5* (Yin *et al*., 2011). Further study of *OsCSLD4* is expected to yield new insights into the role of hemicelluloses in plant development.

Supplementary data

Supplementary data are available at *JXB* online.

Fig. S1. Phylogenetic tree of CSLD proteins in rice (Os), maize (Zm), *Arabidopsis* (At), barley (Hv), sorghum (Sb), and purple false brome (Bradi).

Fig. S2. Comparison of costal cell size in the third-leaf blade of wild-type, *sle1-1*, and *sle1-2* plants.

Fig. S3. Internode elongation patterns in wild-type, *sle1-1* and *sle1-2* mature plants.

Fig. S4. Root phenotypes of wild-type and *sle1* plants.

Fig. S5. Comparison of the number of vascular bundles and the vascular bundle interval in the third-leaf blade among wild-type, *sle1-1*, and *sle1-2* plants.

Fig. S6. Double-target *in situ* hybridization of *OsCLSD4*/*SLE1* counterstained with histone *H4* in a cross-section of shoot apex in wild-type plants.

Fig. S7. Real-time PCR analysis of histone *H4*, *CDKB2;1*, and *OsCSLD4* expression in wild-type, *sle1-1* and *sle1-2* plants.

Fig. S8. Expression pattern of *AtCSLD5* in a cross-section of *Arabidopsis* shoot apex.

Acknowledgements

We would like to express great appreciation to Drs Kazuhiko Nishitani and Ryusuke Yokoyama (Tohoku University) for valuable discussions and advice on our work. We also thank Dr Masaaki Umeda (Nara Institute of Science and Technology) for kindly providing the cDNA of *CDKB2;1*, and Dr Yutaka Sato (Nagoya University) for kind suggestions to help the progress of our work.

References

Bernal AJ, Jensen JK, Harholt J, *et al.* 2007. Disruption of *ATCSLD5* results in reduced growth, reduced xylan and homogalacturonan synthase activity and altered xylan occurrence in *Arabidopsis*. *The Plant Journal* **52,** 791–802.

Bernal AJ, Yoo CM, Mutwil M, Jensen JK, Hou G, Blaukopf C, Sørensen I, Blancaflor EB, Scheller HV, Willats WGT. 2008. Functional analysis of the cellulose synthase-like genes *Csld1*, *Csld2*, and *Csld4* in tip-growing *Arabidopsis* cells. *Plant Physiology* **148,** 1238–1253.

Burton RA, Wilson SM, Hrmova M, Harvey AJ, Shirley NJ, Medhurst A, Stone BA, Newbigin EJ, Bacic A, Fincher GB. 2006. Cellulose synthase-like *CslF* genes mediate the synthesis of cell wall (1,3;1,4)-β-D-glucans. *Science* **311,** 1940–1942.

Cocuron JC, Lerouxel O, Drakakaki G, Alonso AP, Liepman AH, Keegstra K, Raikhel N, Wilkerson CG. 2007. A gene from the cellulose synthase-like C family encodes a β-1,4-glucan synthase. *Proceedings of the National Academy of Sciences, U S A* **104,** 8550–8555.

Doblin MS, Pettolino FA, Wilson SM, Campbell R, Burton RA, Fincher GB, Newbigin E, Bacic A. 2009. A barley cellulose synthase-like *CSLH* gene mediates (1,3;1,4)-beta-D-glucan synthesis in transgenic *Arabidopsis*. *Proceedings of the National Academy of Science, USA* **106,** 5996–6001.

Dwivany FM, Yulia D, Burton RA, Shirley NJ, Wilson SM, Fincher GB, Bacic A, Newbigin E, Doblin MS. 2009. The *Cellulose-synthase like C* (*CslC*) family of barley includes members that are integral membrane proteins targeted to the plasma membrane. *Molecular Plant* **2,** 1025–1039.

Favery B, Ryan E, Foreman J, Linstead P, Boundonck K, Steer M, Shaw P, Dolan L. 2001. *KOJAK* encodes a cellulose synthase-like protein required for root hair cell morphogenesis in *Arabidopsis*. *Genes and Development* **15,** 79–89.

Fincher GB. 2009. Revolutionary times in our understanding of cell wall biosynthesis and remodeling in the grasses. *Plant Physiology* **149,** 27–37.

Hazen SP, Scott-Craig JS, Walton JD. 2002. Cellulose synthase-like genes of rice. *Plant Physiology* **128,** 336–340.

Horiguchi G, Tsukaya H. 2011. Organ size regulation in plants: insights from compensation. *Frontiers in Plant Science* **2,** 1–6.

Hu J, Zhu L, Zeng D, *et al.* 2010. Identification and characterization of *NARROW AND ROLLED LEAF 1*, a novel gene regulating leaf morphology and plant architecture in rice. *Plant Molecular Biology* **73,** 283–292.

Hunter CT, Kirienko DH, Sylvester AW, Peter GF, McCarty DR, Koch KE. 2012. *Cellulose synthase-like* D1 is integral to normal cell division, expansion, and leaf development in maize. *Plant Physiology* **158,** 708–724.

Ji X, Dong B, Shiran B, Talbot MJ, Edlington JE, Hughes T, White RG, Gubler F, Dolferus R. 2011. Control of abscisic acid catabolism and abscisic acid homeostasis is important for reproductive stage stress tolerance in cereals. *Plant Physiology* **156,** 647–662.

Kamiya N, Itoh J, Morikami A, Nagato Y, Matsuoka M. 2003. The *SCARECROW* gene's role in asymmetric cell divisions in rice plants. *The Plant Journal* **36,** 45–54.

Kim CM, Park SH, Je BI, Park SH, Park SJ, Piao HL, Eun MY, Dolan L, Han C. 2007. *OsCsld1*, a cellulose synthase-like D1 gene, is required for root hair morphogenesis in rice. *Plant Physiology* **143,** 1220–1230.

Klindworth DL, Williams ND. 2001. Characterization of a mitotic mutant of durum wheat. Chromosome Research **9,** 377–386.

Kouchi H, Hata S. 1993. Isolation and characterization of novel nodulin cDNAs representing genes expressed at early stages of soybean nodule development. *Molecular and General Genetics* **238,** 106–119.

Kurek I, Kawagoe Y, Jacob-Wilk D, Doblin M, Delmer D. 2002. Dimerization of cotton fiber cellulose synthase catalytic subunits occurs via oxidation of the zinc-binding domains. *Proceedings of the National Academy of Sciences, U S A* **99,** 11109–11114.

Li M, Xiong G, Li R, Cui J, Tang D, Zhang B, Pauly M, Cheng Z, Zhou Y. 2009. Rice cellulose synthase-like D4 is essential for normal cell-wall biosynthesis and plant growth. *The Plant Journal* **60,** 1055–1069.

Liepman AH, Wilkerson CG, Keegstra K. 2005. Expression of cellulose synthase-like (*Csl*) genes in insect cells reveals that *CslA* family members encode mannan synthases. *Proceedings of the National Academy of Sciences, U S A* **102,** 2221–2226.

Lukowitz W, Mayer U, Jügens G. 1996. Cytokinesis in the *Arabidopsis* embryo involves the synthaxin-related *KNOLLE* gene product. *Cell* **84,** 61–71.

Matsui T, Omasa K, Horie T. 1999. Mechanism of anther dehiscence in rice (*Oryza sativa* L.). *Annals of Botany* **84,** 501–506.

Menges M, Hennig L, Gruissem W, Murray JAH. 2003. Genome-wide gene expression in an *Arabidopsis* cell suspension. *Plant Molecular Biology* **53,** 423–442.

Penning BW, Hunter CT III, Tyengwa R, *et al.* 2009. Genetic resources for maize cell wall biology. *Plant Physiology* **151,** 1703–1728.

Richmond TA, Somerville CR. 2000. The cellulose synthase superfamily. *Plant Physiology* **124,** 495–498.

Samuels AL, Giddings TH Jr, Staehelin LA. 1995. Cytokinesis in tobacco BY-2 and root tip cells: a new model of cell plate formation in higher plants. *Journal of Cell Biology* **130,** 1345–1357.

Scheller HV, Ulvskov P. 2010. Hemicelluloses. *Annual Review of Plant Biology* **61,** 263–289.

Söllner R, Glässer G, Wanner G, Somerville CR, Jürgens G, Assaad FF. 2002. Cytokinesis-defective mutants of *Arabidopsis*. *Plant Physiology* **129,** 678–690.

Strompen G, Kasmi FE, Richter S, Lukowitz W, Assaad FF, Jügens G, Mayer U. 2002. The *Arabidopsis HINKEL* gene encodes a kinesin-related protein involved in cytokinesis and is expressed in a cell cycle-dependent manner. *Current Biology* **12,** 153–158.

Suzuki S, Li L, Sun YH, Chiang VL. 2006. The cellulose synthase gene superfamily and biochemical functions of xylem-specific cellulose synthase-like genes in *Populus trichocarpa*. *Plant Physiology* **142,** 1233–1245.

Tamura K, Peterson D, Peterson N, Stecher G, Nei M, and Kumar S. 2011. MEGA5: Molecular Evolutionary Genetics Analysis using maximum likelihood, evolutionary distance, and maximum parsimony methods. *Molecular Biology and Evolution* **28,** 2731–2739.

Taylor NG. 2008. Cellulose biosynthesis and deposition in higher plants. *New Phytologist* **178,** 239–252.

Umeda M, Umeda-Hara C, Yamaguchi M, Hashimoto J, Uchimiya H. 1999. Differential expression of genes for cyclin-dependent protein kinases in rice plants. *Plant Physiology* **119,** 31–40.

Wang X, Cnops G, Vanderhaeghen R, De Block S, Van Montagu M, Van Lijsebettens M. 2001. *AtCSLD3*, a cellulose synthase-like gene important for root hair growth in *Arabidopsis*. *Plant Physiology* **126,** 575–586.

Wu C, Fu Y, Hu G, Si H, Cheng S, Liu W. 2010. Isolation and characterization of a rice mutant with narrow and rolled leaves. *Planta* **232,** 313–324.

Yin L, Verhertbruggen Y, Oikawa A, *et al.* 2011. The cooporative activities of CSLD2, CSLD3, and CSLD5 are required for normal *Arabidopsis* development. *Molecular Plant* doi: 10.1093/mp/ssr026

Zhou S, Wang Y, Li W, *et al.* 2011. *Pollen semi-sterility1* encodes a Kinesin-1-like protein important for male meiosis, anther dehiscence, and fertility in rice. *Plant Cell* **23,** 111–129.

Zuo J, Niu QW, Nishizawa N, Wu Y, Kost B, Chua NH. 2000. KORRIGAN, an *Arabidopsis* endo-1,4-β-glucanase, localizes to the cell plate by polarized targeting and is essential for cytokinesis. *Plant Cell* **12,** 1137–1152.